Peer-Reviewed Technical Communication

Efficient Adaptive Turbo Equalization for Multiple-Input–Multiple-Output Underwater Acoustic Communications

Weimin Duan, Jun Tao, *Member, IEEE*, and Y. Rosa Zheng, *Fellow, IEEE*

***Abstract*—An efficient adaptive turbo equalization (ATEQ) scheme is proposed for multiple-input–multiple-output underwater acoustic (UWA) communications. The proposed ATEQ scheme utilizes two layers of iterative processing: The inner-layer iteration is the soft-decision-based equalizer parameters adaptation and filtering of received signals in the equalizer, and the outer-layer iteration is the Turbo exchange of extrinsic log-likelihood ratio between the equalizer and decoder. In contrast, the existing ATEQ schemes use hard-decision symbols for filter adaptation but soft symbols for filtering and Turbo iteration. When the adaptive filters are designed and updated via the normalized least mean squares (NLMS) or the improved proportionate NLMS algorithms for low computational complexity and good channel tracking, the soft symbols utilized in both the pilot-assisted and the decision-directed modes of the proposed ATEQ scheme achieve fast convergence with short training sequences, thus achieving high spectrum efficiency. The proposed scheme is evaluated by the field trail data collected in the 2008 Surface Processes and Acoustic Communications Experiment. The results demonstrate that the proposed ATEQ scheme is robust against the severe triply-selective UWA channels and mitigate slow-convergence problem commonly suffered by direct-adaptation equalizers.**

***Index Terms*—Adaptive equalization, *a posteriori* soft decision (SD), data reuse, improved proportionate normalized least mean squares (IPNLMS), multiple-input–multiple-output (MIMO), normalized least mean squares (NLMS), turbo equalization, underwater acoustic (UWA) communication.**

Manuscript received April 16, 2016; revised October 27, 2016 and March 17, 2017; accepted May 18, 2017. The work of W. Duan and Y. R. Zheng was supported in part by the National Science Foundation under Grant ECCS-1408316. The work of J. Tao was supported in part by the Open Project Program of the Key Laboratory of Underwater Acoustic Signal Processing of Ministry of Education, Southeast University, Nanjing, China, under Grant UASP1601, in part by the Foundation of Key Laboratory of System Control and Information Processing, Ministry of Education, China, under Grant Scip201610, and in part by the Fundamental Research Funds for the Central Universities under Grant 2242016K30013. *(Corresponding author: Weimin Duan.)*

Associate Editor: J. Gomes.

W. Duan was with the Department of Electrical and Computer Engineering, Missouri University of Science and Technology, Rolla, MO 65409 USA. He is now with Qualcomm Technologies, Inc., San Diego, CA 92121 USA (e-mail: wdrgc@mst.edu).

J. Tao is with the Key Laboratory of Underwater Acoustic Signal Processing of Ministry of Education, Southeast University, Nanjing 210096, China and also with the Key Laboratory of System Control and Information Processing, Ministry of Education of China, Shanghai 200240, China (e-mail: jtao@seu.edu.cn).

Y. R. Zheng is with the Department of Electrical and Computer Engineering, Missouri University of Science and Technology, Rolla, MO 65409 USA (e-mail: zhengyr@mst.edu).

Digital Object Identifier 10.1109/JOE.2017.2707285

I. Introduction

MULTIPLE-INPUT–MULTIPLE-OUTPUT (MIMO) underwater acoustic (UWA) communication exhibits unique technical challenges due to the triply selective property of the underlying MIMO UWA channel, for which the transmit signal simultaneously experiences the frequency selectivity, the time selectivity, and the spatial selectivity [1]. The frequency selectivity and the time selectivity are generally very severe, for the extremely long delay spread and the rapid dynamics of the UWA channel. For example, a medium-range horizontal UWA channel can have a delay spread of several tens of milliseconds spanning several tens or even hundreds of symbol periods, and the channel coherence time is typically several tens of milliseconds. Further, the spatial selectivity leads to different gains among different transmit and receive elements [2], adding to the difficulty of signal detection.

The harsh MIMO UWA channel demands for powerful signal detection techniques, and turbo equalization has long been recognized as one such promising detection scheme. Turbo equalization typically consists of two components: a soft-input soft-output equalizer and a soft-input soft-output decoder, which iteratively exchange extrinsic information to improve the detection performance. The turbo equalization applied to the UWA communications falls into two classes: The channel-estimation-based turbo equalization (CE-TEQ) [3]–[7] and the adaptive turbo equalization (ATEQ) with no need of explicit channel knowledge [8]–[13]. The equalizer for a CE-TEQ can be a minimum mean square error (MMSE) linear equalizer [3], [4] or a MMSE decision-feedback equalizer [5]–[7], where the calculation of the MMSE equalizer coefficients requires the knowledge of the UWA channel. Since the length of the UWA channel is usually long, the computation of the equalizer coefficients involves a large-dimension matrix inversion, leading to high complexity. The complexity can be further amplified when a MIMO system with multiple transducers and hydrophones is deployed, due to the increased size of the covariance matrix to be inverted. The high complexity means a long signal processing delay, making the CE-TEQ impractical for real-time applications. On the other hand, an ATEQ takes the advantage of low complexity achieved by directly adjusting the equalizer coefficients without any matrix inversion operation. An ATEQ generally achieves suboptimal performance by approaching that of the Wiener filtering and demands for fine parameter

tuning (which is nontrivial for MIMO UWA communication due to the abundant equalizer taps to be adapted) so as to make the adaptive equalizer converge.

A soft-input–soft-output equalizer adopted in the ATEQ typically consists of two filters: A feedforward filter with the received samples as its input, and a soft interference cancelation (SIC) filter whose input is the estimation of transmit symbols [11]–[13]. The adaption of the feedforward filter and the SIC filter, as well as the quality of the SIC filter input are the keys for the success of the ATEQ. In training mode, the filter adaptation and the SIC formulation are routine procedures since the reference symbols are *a priori* perfectly known. It is during the decision directed (DD) phase, diverse filter adaptation and SIC formulation methods are proposed, leading to different ATEQ schemes of different performance [11]–[15]. In [12]–[14], the hard decision on the equalizer output is used to drive the filter adaptation, and the SIC input is the *a priori* soft symbol estimation from the channel decoder. In [11], a similar filter adaptation and SIC formulation scheme as in [12]–[14] is adopted. The difference is that it also takes advantage of the data reuse technique originated in [16]. By data reuse, the filter adaptation and symbol detection are repeated several times over the same set of data, and this helps to improve the detection performance as well as to speed up the filter convergence. Therefore, it shortens the training sequence and improves the transmission efficiency. In [15], hard decisions of the *a priori* soft symbol estimations from the decoder are delivered as the SIC filter input. Different from [11]–[14], the decoder *a priori* soft decisions (SDs) are also incorporated into the filter adaptation, aiming to mitigate the error propagation (EP) effect of hard decisions. However, the scheme still requires a very long training sequence for the initialization of the equalizer. Finally, it is noted most existing works on ATEQ for UWA communication deal with single-input–multiple-output transmissions [12]–[15], and the only MIMO result reported is for the two-transducer scenario with a low-order QPSK modulation [11].

In this paper, an efficient ATEQ is proposed for MIMO UWA communication, with multiple transmit elements and multilevel modulations such as 8PSK and 16QAM. The proposed scheme adopting the low-complexity normalized least mean squares (NLMS) algorithm as well as the improved proportionate normalized least mean squares (IPNLMS) algorithm, still benefits from the data reuse technique [11]. Compared with existing ATEQ schemes, the proposed scheme is improved in both filter adaptation and SIC formulation, achieved by making use of the *a posteriori* SD (at the equalizer output), available in the data reuse iteration. The *a posteriori* SDs have better fidelity than the *a priori* SDs, due to the extra information gleaned in the equalization process. Moreover, the *a posteriori* SDs are utilized in a blockwise way, leading to low complexity and high performance [17]. The proposed ATEQ scheme is tested by extensive experimental data collected in the 2008 Surface Processes and Acoustic Communications Experiment (SPACE08). The low-complexity NLMS algorithm and the sparsity enhanced IPNLMS algorithm are adopted in the data processing. Attributed to the improvement made, the proposed scheme not only achieves error-free detection for most QPSK packets in the MIMO transmission with up to three transmit elements, but also works decently in the MIMO transmission with multilevel modulations such as 8PSK and 16QAM, as shown by the experimental results. Furthermore, relatively short training sequences were found to be sufficient, thereby improvements in the transmission efficiency are realized.

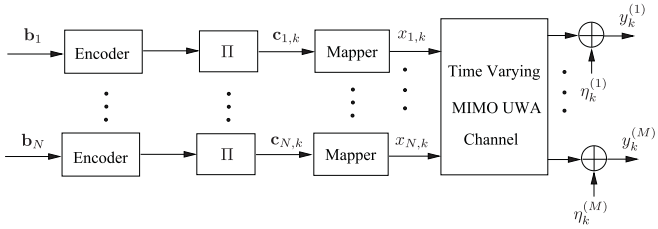

Fig. 1. Block diagram of a MIMO UWA communication system (Π denotes an interleaver).

Notation: The superscripts $(\cdot)^*$, $(\cdot)^T$, and $(\cdot)^H$ represent, respectively, the conjugate, the matrix transpose, and the matrix Hermitian, and $\mathbb{E}\{\cdot\}$ denotes the statistical expectation. The function $\tanh(x)$ denotes the hyperbolic tangent, and the matrix $\mathrm{diag}\{d_1, d_2, \cdots, d_j\}$ is a $j \times j$ diagonal matrix with diagonal elements $d_1, d_2, \ldots, d_j$.

II. System Description and ATEQ Preliminary

A. System Description

An $N \times M$ single-carrier MIMO UWA communication system with spatial multiplexing is considered, where N and M are the number of transducers and the number of hydrophones, respectively. The system diagram is depicted in Fig. 1 where on the transmitter side, the incoming information bits are serial-to-parallel converted into N parallel streams $\{\mathbf{b}_n\}_{n=1}^N$, transmitted by the N transducers. On the nth transmit branch, the information bits are encoded and interleaved. Every q interleaved bits, $\mathbf{c}_{n,k} \triangleq [c_{n,k}^1 \quad c_{n,k}^2 \ldots c_{n,k}^q]$, are mapped to one modulation symbol $x_{n,k}$ taken from a 2^q-ary constellation set $S = \{\alpha_1, \alpha_2, \ldots, \alpha_{2^q}\}$. A given constellation point α_i is mapped to a predetermined bit pattern $\mathbf{s}_i = [s_{i,1} \ s_{i,2} \cdots s_{i,q}]$ with $s_{i,j} \in \{0, 1\}$.

The received baseband signal on the mth hydrophone element at the time k is given by

$$y_k^{(m)} = \sum_{n=1}^{N} \sum_{l=0}^{L-1} h_{l,k}^{(m,n)} x_{n,k-l} + \eta_k^{(m)} \tag{1}$$

where $h_{l,k}^{(m,n)}$ denotes the lth tap of the length-L equivalent channel between the nth transducer element and the mth hydrophone element at time instant k, and $\eta_k^{(m)}$ is the additive noise. Stacking up the receive samples of the M hydrophone as $\mathbf{y}_k = [y_k^{(1)}, y_k^{(2)}, \ldots, y_k^{(M)}]^T$, one has the space-time representation as

$$\mathbf{y}_k = \sum_{l=0}^{L-1} \mathbf{h}_{l,k} \mathbf{x}_{k-l} + \boldsymbol{\eta}_k \tag{2}$$

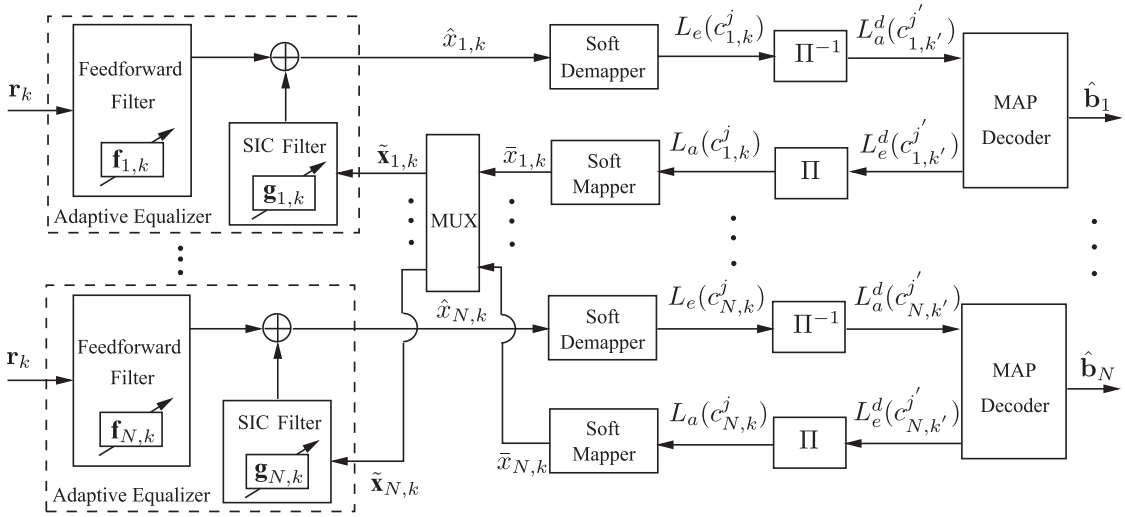

Fig. 2. Structure of the ATEQ for MIMO systems.

where

$$\mathbf{x}_k = [x_{1,k}, x_{2,k}, \ldots, x_{N,k}]^T \tag{3}$$

$$\boldsymbol{\eta}_k = [\eta_k^{(1)}, \eta_k^{(2)}, \ldots, \eta_k^{(M)}]^T \tag{4}$$

$$\mathbf{h}_{l,k} = \begin{bmatrix} h_{l,k}^{(1,1)} & h_{l,k}^{(1,2)} & \cdots & h_{l,k}^{(1,N)} \\ h_{l,k}^{(2,1)} & h_{l,k}^{(2,2)} & \cdots & h_{l,k}^{(2,N)} \\ \vdots & \vdots & \ddots & \vdots \\ h_{l,k}^{(M,1)} & h_{l,k}^{(M,2)} & \cdots & h_{l,k}^{(M,N)} \end{bmatrix}. \tag{5}$$

B. ATEQ for MIMO systems

The structure of the ATEQ for MIMO systems is depicted in Fig. 2, where the adaptive equalizer consists of two units: The feedforward filtering unit and the SIC unit. In most existing adaptive equalizers, the SIC is performed with the *a priori* SD $\bar{x}_{n,k}$, calculated with the bit *a priori* log likelihood ratio (LLR) $L_a(c^j_{n,k})$ from the decoder as

$$\bar{x}_{n,k} = \mathbb{E}\left[x_{n,k} | \left\{L_a\left(c^j_{n,k}\right)\right\}_{j=1}^{q}\right] = \sum_{\alpha_i \in S} \alpha_i P, \quad x_{n,k} = \alpha_i \tag{6}$$

where

$$P\left(x_{n,k} = \alpha_i\right) = \prod_{j=1}^{q} \frac{1}{2}\left(1 + \tilde{s}_{i,j} \tanh\left(L_a\left(c^j_{n,k}\right)/2\right)\right) \tag{7}$$

with

$$\tilde{s}_{i,j} = \begin{cases} +1, & \text{if } \mathrm{s_{i,j}} = 0 \\ -1, & \text{if } \mathrm{s_{i,j}} = 1. \end{cases}$$

The equalizer output is given as

$$\hat{x}_{n,k} = \mathbf{f}_{n,k}^H \mathbf{r}_k + \mathbf{g}_{n,k}^H \tilde{\mathbf{x}}_{n,k} \tag{8}$$

where $\mathbf{r}_k = [\mathbf{y}^T_{k+K_1}, \ldots, \mathbf{y}^T_{k-K_2}]^T$, and $\tilde{\mathbf{x}}_{n,k} = [(\bar{\mathbf{x}}_{n,k-K_3})^T, \ldots, (\bar{\mathbf{x}}_{n,k})^T \ldots, (\bar{\mathbf{x}}_{n,k+K_4})^T]^T$ with $\bar{\mathbf{x}}_{n,k'} = [\bar{x}_{1,k'}, \bar{x}_{2,k'}, \ldots, \bar{x}_{N,k'}]^T$ when $k' \neq k$, and $\bar{\mathbf{x}}_{n,k'} = [\bar{x}_{1,k'}, \ldots, \bar{x}_{n-1,k'}, 0, \bar{x}_{n+1,k'}, \ldots, \bar{x}_{N,k'}]^T$ when $k' = k$. The parameters K_1, K_2, K_3, K_4 are nonnegative integers. Obviously, the length of the feedforward filter and the length of the SIC filter are $M(K_1+K_2+1)$ and $N(K_3+K_4)$, respectively, leading to a combined filter length of $K_{eq} = M(K_1+K_2+1)+N(K_3+K_4)$. It is noted K_{eq} is the number of taps for a particular transmit stream, and the total number of taps for the adaptive equalizer shall be scaled by a factor of N. For notation convenience, one expresses (8) as

$$\hat{x}_{n,k} = \mathbf{w}_{n,k}^H \mathbf{u}_k \tag{9}$$

where

$$\mathbf{w}_{n,k} = [\mathbf{f}_{n,k}^T \;\; \mathbf{g}_{n,k}^T]^T \tag{10}$$

$$\mathbf{u}_k = [\mathbf{r}_k^T \;\; \tilde{\mathbf{x}}_{n,k}^T]^T \tag{11}$$

The ATEQ usually works in both training mode and DD mode, and the NLMS algorithm is used as an example without loss of generality. In the training mode, the adaptation of the equalizer vector is as follows:

$$\mathbf{w}_{n,k+1} = \mathbf{w}_{n,k} + \frac{\mu(x_{n,k} - \hat{x}_{n,k})^* \mathbf{u}_k}{\delta_{\mathrm{NLMS}} + \mathbf{u}_k^H \mathbf{u}_k}, \qquad 1 \leq k \leq K_p \tag{12}$$

where μ is the step size, δ_{NLMS} is a small number for regularizing the adaptation at the initial stage, $x_{n,k}$ is the training symbol known *a priori*, and K_p is the length of the training sequence.

In the DD mode, the updating of the equalizer vector is as follows:

$$\mathbf{w}_{n,k+1} = \mathbf{w}_{n,k} + \frac{\mu(Q(\hat{x}_{n,k}) - \hat{x}_{n,k})^* \mathbf{u}_k}{\delta_{\mathrm{NLMS}} + \mathbf{u}_k^H \mathbf{u}_k}, \qquad K_p < k \leq K_b \tag{13}$$

where $Q(\hat{x}_{n,k})$ denotes the tentative hard decision on the equalizer output, and K_b is the length of each processed block.

As mentioned earlier, the length of the concatenated feedforward filter and the SIC filter is $K_{eq} = M(K_1+K_2+1)+N(K_3+K_4)$. Due to the long delay spread of the underwater channel as well as the multiple transmit and receive elements, the number of equalizer taps to be adapted is large. To make

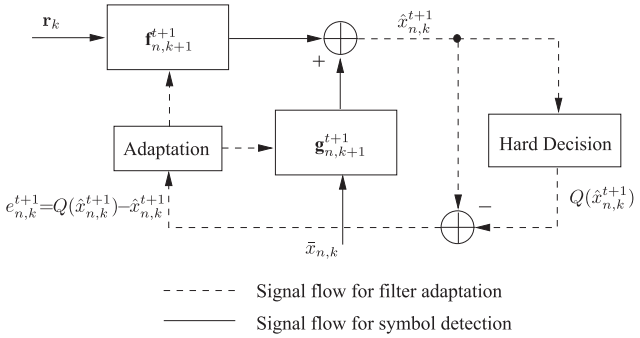

Fig. 3. Block diagram of the hard-decision adaptive equalizer with data reuse.

the adaptive equalizer converge, a long training sequence is required, which sacrifices the transmission efficiency. To avoid long training sequence, the data reuse technique has been applied in the hard-decision directed adaptive turbo equalization (HD-ATEQ) [11] and the iterative CE-TEQ [4]. The hard-DD equalizer adaptation with data reuse is demonstrated in Fig. 3, where the tap updating is repeated over the same block of received signals for a couple of times as follows:

$$\mathbf{w}_{n,k+1}^{t+1} = \mathbf{w}_{n,k}^{t+1} + \frac{\mu(Q(\hat{x}_{n,k}^{t+1}) - \hat{x}_{n,k}^{t+1})^* \mathbf{u}_k}{\delta_{\text{NLMS}} + \mathbf{u}_k^H \mathbf{u}_k}, \quad K_p < k \le K_b, t \ge 0 \tag{14}$$

where the superscript $t+1$ denotes the $(t+1)$th round of data reuse, and $\hat{x}_{n,k}^{t+1} = \mathbf{w}_{n,k}^{t+1\,H} \mathbf{u}_k$. The purpose of using $t+1$ as the index of the data reuse round is for the convenience of comparison with the proposed equalizer adaptation, as shown shortly. The adaptation of the equalizer vector $\mathbf{w}_{n,k+1}^0$ at the zeroth round of data reuse is actually the same as that of (14). It is noted that $\mathbf{w}_{n,1}^{t+1} = \mathbf{w}_{n,K_b+1}^t$. The HD-ATEQ [11] may suffer the EP, which is highly possible in practical UWA communication [4]. When the EP happens, its effect can be catastrophic for turbo equalization. Moreover, the input of the SIC filter remains unchanged over the multiple rounds of data reuse [11].

As demonstrated in Fig. 2, the equalized symbol $\hat{x}_{n,k}$ is translated into the extrinsic bit LLRs $L_e(c_{n,k}^j)$, which are deinterleaved and input as the *a priori* LLRs $L_a^d(c_{n,k'}^{j'})$ of the maximum *a posteriori* probability decoder. After decoding, the decoder outputs its extrinsic LLRs $L_e^d(c_{n,k'}^{j'})$, which (after interleaving) are fed back to the equalizer as its *a priori* LLR input $L_a(c_{n,k}^j)$. The extrinsic information are exchanged between the equalizer and the decoder iteratively, with its reliability increasing with the number of iterations. Once the iterative procedure is finished, the hard decisions on the information bits $\hat{\mathbf{b}}_n$ are made.

III. Proposed ATEQ

In this work, an efficient ATEQ scheme is proposed, by performing the equalizer adaptation and the SIC with the *a posteriori* SDs available due to the data reuse, as demonstrated in Fig. 4. For notation convenience, the proposed soft-decision-driven adaptive turbo equalization is called the SD-ATEQ. There are two layers of iterative processing in the proposed ATEQ: The outer-layer iteration between the equalizer and decoder, and the inner-layer iteration (data reuse) inside the adaptive equalizer itself. For convenience, the outer-layer iteration is called "turbo iteration," and the inner-layer iteration is named as "equalizer iteration." It is pointed out that the *a posteriori* SDs are fed back in a block-wise way inside the adaptive equalizer, which improves the robustness and performance of the ATEQ as well as reduces the complexity [17]. In the following, the computation of the *a posteriori* SD is first presented, then the *a posteriori* SD-based equalizer adaptation and SIC are detailed.

A. A Posteriori SD Computation in the Equalizer Iterations

At the tth ($t \ge 0$) round of equalizer iteration, the *a posteriori* SD $\check{x}_{n,k}^t$ of the equalized symbol $\hat{x}_{n,k}^t$ is calculated as

$$\check{x}_{n,k}^t = \sum_{\alpha_i \in S} \alpha_i P\left(x_{n,k} = \alpha_i | \hat{x}_{n,k}^t\right) \tag{15}$$

where the *a posteriori* probability $P(x_{n,k} = \alpha_i | \hat{x}_{n,k}^t)$ is given as

$$P\left(x_{n,k} = \alpha_i | \hat{x}_{n,k}^t\right) = \frac{p\left(\hat{x}_{n,k}^t | x_{n,k} = \alpha_i\right) P\left(x_{n,k} = \alpha_i\right)}{p\left(\hat{x}_{n,k}^t\right)}. \tag{16}$$

The *a priori* probability $P(x_{n,k} = \alpha_i)$ is computed with the *a priori* LLRs as in (7), and $p(\hat{x}_{n,k}^t)$ is obtained via the normalization $\sum_{i=1}^{2^q} P(x_{n,k} = \alpha_i | \hat{x}_{n,k}^t) = 1$. The equalizer output $\hat{x}_{n,k}^t$ conditioned on $x_{n,k} = \alpha_i$ is assumed to follow a Gaussian distribution [18]–[20], as

$$p\left(\hat{x}_{n,k}^t | x_{n,k} = \alpha_i\right) = \frac{1}{\pi \delta_n^t} \exp\left\{ -\frac{|\hat{x}_{n,k}^t - \mu_n^t \alpha_i|^2}{\delta_n^t} \right\} \tag{17}$$

where

$$\mu_n^t = \frac{1}{K_d} \sum_{k=K_p+1}^{K_b} \frac{\hat{x}_{n,k}^t}{Q(\hat{x}_{n,k}^t)} \tag{18}$$

$$\delta_n^t = \frac{1}{K_d} \sum_{k=K_p+1}^{K_b} |\hat{x}_{n,k}^t - \mu_n^t Q(\hat{x}_{n,k}^t)|^2 \tag{19}$$

with $K_d = K_b - K_p$ being the length of information block. Obviously, the evaluation of μ_n^t and δ_n^t relies on the entire block of estimated symbols. As a result, the *a posteriori* SDs are unavailable until all symbols in the block are equalized. This fact naturally leads to the block-wise SD feedback operation, where the *a posteriori* SD $\check{x}_{n,k}^t$ of the tth equalizer iteration is used in the $(t+1)$th equalizer iteration, as shown in Fig. 4. Over equalizer iterations, the reliability of the *a posteriori* SD $\check{x}_{n,k}^t$ keeps increasing thus speeds up the convergence of the equalizer. The block-wise SD feedback mechanism has shown the advantage of low complexity and high performance [17].

B. A Posteriori SD-Based Equalizer Adaptation and SIC

1) A Posteriori SD-Based Equalizer Adaptation: At the $(t+1)$th equalizer iteration, the block of *a posteriori* SDs from

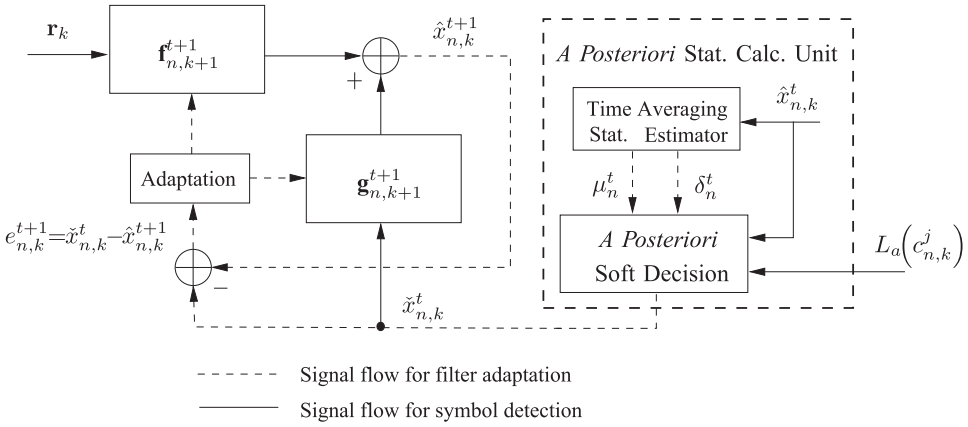

Fig. 4. Block diagram of the proposed adaptive equalizer with data reuse.

the tth equalizer iteration $\{\breve{x}_{n,k}^{t}\}_{k=K_p+1}^{K_b}$ are fed into the filter adaptation unit, and the equalizer vector is updated as

$$\mathbf{w}_{n,k+1}^{t+1}=\mathbf{w}_{n,k}^{t+1}+\frac{\mu(\breve{x}_{n,k}^{t}-\hat{x}_{n,k}^{t+1})^{*}\mathbf{u}_k}{\delta_{\mathrm{NLMS}}+\mathbf{u}_k^H\mathbf{u}_k},\qquad t\geq 0. \tag{20}$$

The equalizer adaption at the zeroth equalizer iteration is different from (20), since there are no *a posteriori* SDs available. When the number of turbo iteration $N_{\mathrm{iter}}>0$, the *a priori* SDs $\{\bar{x}_{n,k}\}_{k=K_p+1}^{K_b}$ are instead used for the equalizer adaptation. When $N_{\mathrm{iter}}=0$, even the *a priori* SD $\bar{x}_{n,k}$ is unavailable, so the hard-DD equalizer adaptation as (14) is adopted. In summary, one has the following equalizer adaptation at the zeroth equalizer iteration:

$$\mathbf{w}_{n,k+1}^{0}=\begin{cases}\mathbf{w}_{n,k}^{0}+\dfrac{\mu(\bar{x}_{n,k}-\hat{x}_{n,k}^{0})^{*}\mathbf{u}_k}{\delta_{\mathrm{NLMS}}+\mathbf{u}_k^H\mathbf{u}_k}, & N_{\mathrm{iter}}>0\\ \mathbf{w}_{n,k}^{0}+\dfrac{\mu(Q(\hat{x}_{n,k}^{0})-\hat{x}_{n,k}^{0})^{*}\mathbf{u}_k}{\delta_{\mathrm{NLMS}}+\mathbf{u}_k^H\mathbf{u}_k}, & N_{\mathrm{iter}}=0.\end{cases} \tag{21}$$

Finally, the training-mode equalizer adaptation as given by (12) is performed at each equalizer iteration of the data reuse procedure.

The sparsity enhanced IPNLMS algorithm has also been adopted to process the experimental data. The IPNLMS proportionately adapts the equalizer vector as

$$\mathbf{w}_{n,k+1}^{t+1}=\mathbf{w}_{n,k}^{t+1}+\frac{\mu(\breve{x}_{n,k}^{t}-\hat{x}_{n,k}^{t+1})^{*}\mathbf{G}_{n,k}\mathbf{u}_k}{\mathbf{u}_k^H\mathbf{G}_{n,k}\mathbf{u}_k+\delta_{\mathrm{IPNLMS}}},\qquad t\geq 0 \tag{22}$$

and

$$\mathbf{w}_{n,k+1}^{0}=\begin{cases}\mathbf{w}_{n,k}^{0}+\dfrac{\mu(\bar{x}_{n,k}-\hat{x}_{n,k}^{0})^{*}\mathbf{G}_{n,k}\mathbf{u}_k}{\mathbf{u}_k^H\mathbf{G}_{n,k}\mathbf{u}_k+\delta_{\mathrm{IPNLMS}}}, & N_{\mathrm{iter}}>0\\ \mathbf{w}_{n,k}^{0}+\dfrac{\mu(Q(\hat{x}_{n,k}^{0})-\hat{x}_{n,k}^{0})^{*}\mathbf{G}_{n,k}\mathbf{u}_k}{\mathbf{u}_k^H\mathbf{G}_{n,k}\mathbf{u}_k+\delta_{\mathrm{IPNLMS}}}, & N_{\mathrm{iter}}=0\end{cases} \tag{23}$$

where δ_{IPNLMS} is a small positive number for regularization, and $\mathbf{G}_{n,k}=\mathrm{diag}\ \{g_{n,k}(0),g_{n,k}(1),\ldots,g_{n,k}(K_{eq}-1)\}$ is a diagonal proportionate matrix with the $l^{'}$th diagonal element given by

$$g_{n,k}(l^{'})=\frac{1-\alpha}{2K_{eq}}+(1+\alpha)\frac{|\mathbf{w}_{n,k}^{t+1}(l^{'})|}{2\|\mathbf{w}_{n,k}^{t+1}\|_1+\epsilon},\qquad 0\leq l^{'}\leq K_{eq}-1 \tag{24}$$

where ϵ is also a regularization parameter introduced to avoid numerical instability, $\mathbf{w}_{n,k}^{t+1}(l^{'})$ is the $l^{'}$th element of $\mathbf{w}_{n,k}^{t+1}$, and $|\cdot|$ and $\|\cdot\|_1$ are the absolute operator and the l_1-norm operator, respectively. The selection of α depends on the sparsity of the equalizer. When $\alpha=-1$, the IPNLMS reduces to the NLMS [21] and the equalizer sparsity is not exploited. When $\alpha=1$, the IPNLMS behaves such as the proportionate normalized least mean squares (PNLMS) [22]. It is noted that the IPNLMS is still of linear complexity without involving any matrix inversion operation.

2) A Posteriori SD-Based SIC Scheme: The performance of the SIC depends heavily on the quality of the SD. Most ATEQ schemes employ the *a priori* SDs for SIC [11]–[14]. By utilizing the *a posteriori* SDs, which possess higher fidelity than the *a priori* SDs due to the extra information gleaned in the equalization process, one is able to improve the SIC. Specifically, with the improved SIC, the equalizer output $\hat{x}_{n,k}^{t+1}$ is given by

$$\hat{x}_{n,k}^{t+1}=\mathbf{f}_{n,k}^{t+1\,H}\mathbf{r}_k+\mathbf{g}_{n,k}^{t+1\,H}\breve{\mathbf{x}}_{n,k}^{t}. \tag{25}$$

Obviously, the *a priori* SDs $\tilde{\mathbf{x}}_{n,k}$ in (8) have been replaced with the *a posteriori* SDs $\breve{\mathbf{x}}_{n,k}^{t}=[(\breve{\mathbf{x}}_{n,k-K_3}^{t})^T,\ldots,(\breve{\mathbf{x}}_{n,k}^{t})^T,\ldots,(\breve{\mathbf{x}}_{n,k+K_4}^{t})^T]^T$, where $\breve{\mathbf{x}}_{n,k'}^{t}=[\breve{x}_{1,k'}^{t},\breve{x}_{2,k'}^{t},\ldots,\breve{x}_{N,k'}^{t}]^T$ when $k^{'}\neq k$, and $\breve{\mathbf{x}}_{n,k'}^{t}=[\breve{x}_{1,k'}^{t},\ldots,\breve{x}_{n-1,k'}^{t},0,\breve{x}_{n+1,k'}^{t},\ldots,\breve{x}_{N,k'}^{t}]^T$ when $k^{'}=k$.

IV. Undersea Experimental Results

The proposed adaptive turbo detection scheme has been tested by field trial data collected in the SPACE08 undersea experiment, conducted off the coast of Martha's Vineyard, Edgartown, MA, USA, in October 2008. The water depth of this sea trial was about 15 m. On the transmitter side, four transducers numbered

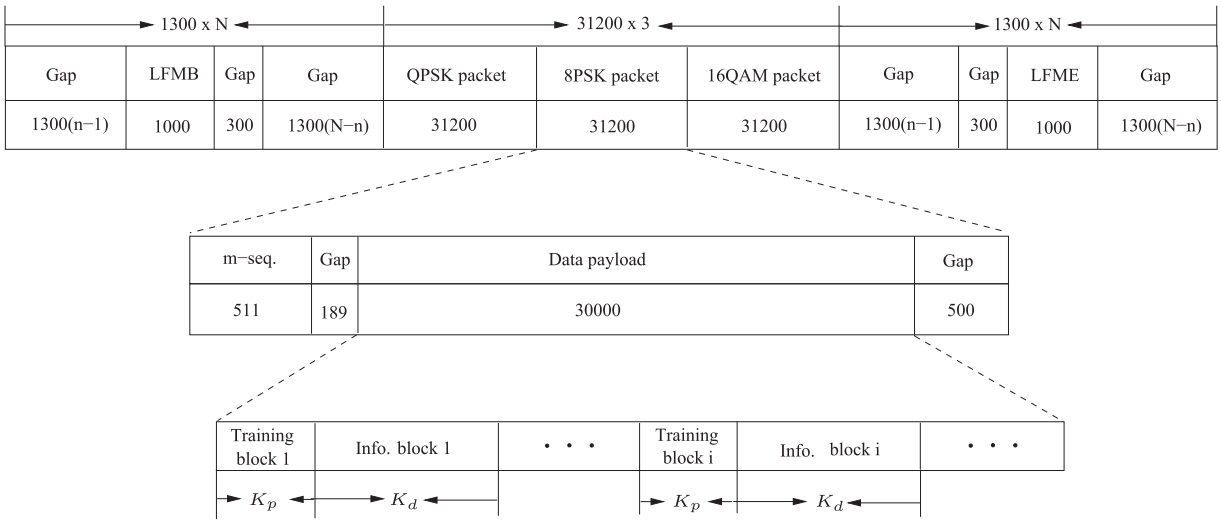

Fig. 5. Format of the transmit signal on the nth transducer in the SPACE08 experiment.

TABLE I
DESCRIPTION OF THE HYDROPHONE ARRAYS

Rx Array name/type	Range (m)	Orientation	Number of hydrophones	Hydrophone spacing (cm)
S1/Cross	60	Southeast	16	3.75
S2/Cross	60	Southwest	16	3.75
S3/Vertical	200	Southeast	24	5
S4/Vertical	200	Southwest	24	5
S5/Vertical	1000	Southeast	12	12
S6/Vertical	1000	Southwest	12	12

0 to 3 were deployed. Transducer 0 was fixed on a stationary tripod about 4 m above the ocean bottom. Transducers 1–3 were evenly mounted on a vertical array with 50-cm spacing, and the top transducer in the array was about 3 m above the ocean bottom. Six hydrophone arrays placed at different locations were deployed for signal reception, with detailed information given in Table I. The communication distances were 60, 200, and 1000 m. The top hydrophone of each array was approximately 3.3 m above the sea bottom.

For MIMO transmission, the horizontal encoding scheme [23] with bit-interleaved coded modulation (BCIM) in time domain was adopted at the transmitter, as shown in Fig. 1. The channel coding was a rate $R_c = 1/2$ convolutional code with generator polynomial [17, 13] in octal notation. The modulations include QPSK, 8PSK, and 16QAM. The transmission power for all modulation schemes were the same, so detection becomes more difficult when the modulation level increases. The carrier frequency was $f_c = 13$ kHz and the symbol rate was 9.77 ks/s. A square-root raised cosine filter with a roll-off factor of 0.2 was used for pulse shaping, leading to the occupied channel bandwidth of about 11.72 kHz. At the receiver side, the passband sampling rate was 39.0625 kHz.

The signal format at the nth transducer is illustrated in Fig. 5, where the transmit burst starts with a header linear frequency modulation (LFM) signal named LFMB and ends with a trailing LFM signal named LFME. The LFM signals are used for coarse synchronization and channel structure measurement. With the signaling structure in Fig. 5, the LFM signals for different transducers avoid interfering each other by nonoverlapping in time. Following the header LFM signal are three data packets with QPSK, 8PSK, and 16QAM modulations, each starts with a BPSK-modulated m-sequence of length 511 for doppler shift estimation, followed by a data payload consisting of 30 000 symbols. The use of long data payload improves the transmission efficiency. Gaps are inserted in the transmission burst, and they can be used for estimating the noise power. With the estimated noise power, the signal-to-noise ratio (SNR) can also be evaluated. For the SPACE08 experiment, the typical SNR estimation is in the range of 20 to 32 dB.

The received bursts of the 200-m channel and the 1000-m channel are shown in Fig. 6. Obviously, the strength of the 200-m signal (peak-to-peak amplitude of 0.38) is much stronger than the 1000-m signal (peak-to-peak amplitude of 0.038), which is reasonable since the acoustic signal attenuates with distance. Besides, impulsive interference is observed in the 1000-m signal.

In Fig. 7, the channel impulse response (CIR) measured in the experiment is shown for both the 200-m transmission and the 1000-m transmission, where "T#" and "H#" denote the indices of the transducer and the hydrophone, respectively. The following observations are made: First, the multipath energy spread over a time window of 10 ms, corresponding to a channel length of 100 taps in terms of the symbol period $T_s = 0.1024$ ms; second, the channels are nonminimum phase as the strongest multipath component is not at the very beginning of the CIR, which add to the difficulty for equalization; third, the channel is fast time varying, especially for the 200-m channel, making the adaptive symbol detection quite challenging.

A. Parameters Setup

Due to the fast time variations of the UWA channels, the adaptive turbo detector partitions each long data payload into multiple blocks of size K_b for processing, as shown in Fig. 5. For

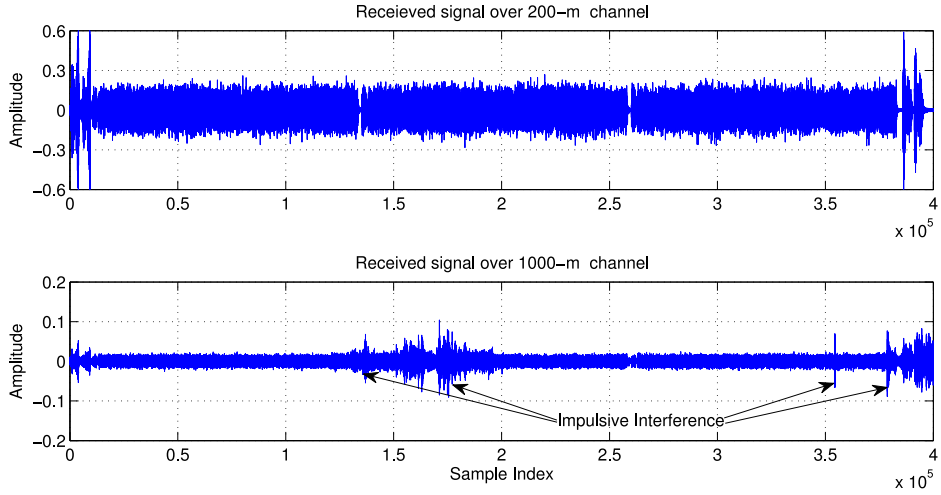

Fig. 6. Example of the received signals in 200 and 1000-m transmissions.

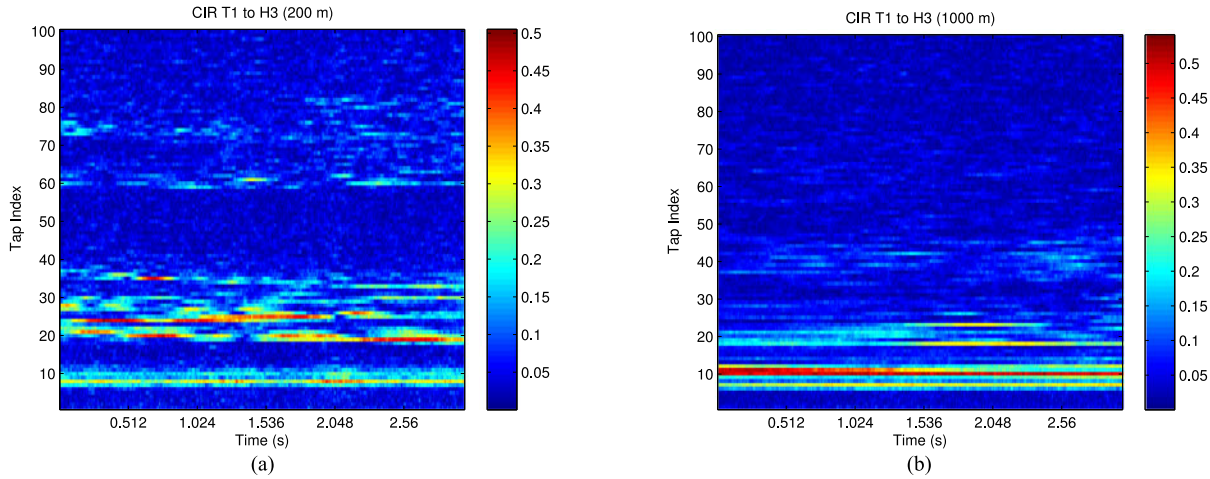

Fig. 7. Example of the CIRs over a period of time.

TABLE II
TRAINING OVERHEADS AND THE CORRESPONDING INFORMATION RATES FOR DIFFERENT COMBINATIONS OF MODULATION AND MIMO SIZE

Modulation	MIMO size	Block size (K_b)	Training overhead (ξ)	Information rate (kb/s)
QPSK	2×6	3600	13.89%	16.82
	3×12	2200	22.73%	22.64
	4×12	1800	27.78%	28.22
8PSK	2×6	2200	22.73%	22.64
	3×12	1800	27.78%	31.74
	4×12	1200	41.76%	34.18
16QAM	2×6	1800	27.78%	28.22
	3×12	1500	33.33%	39.06
	4×12	1050	47.62%	**40.92**

each partition block, the first K_p symbols are used as the training symbols to initialize the adaptive receiver, and the remaining K_d symbols carries information bits. The resulting training overhead is $\xi = K_p/(K_p + K_d)$ and the corresponding information rate is $9.77 \times \xi q N R_c$ kb/s. In the data processing, K_p is fixed as 500 and the choice of K_d is flexible depending on the modulation and the MIMO size. In Table II, the choice of the training overheads (equivalent to the choice of K_b since K_p is fixed) and the corresponding information rates are summarized, for different combinations of modulation and MIMO size.

TABLE III
TOTAL NUMBER OF PACKETS ACHIEVING THE SPECIFIED BER LEVEL (2×6 MIMO)

Range	# of turbo iter.	QPSK (BER $= 0$)		8PSK (BER $< 10^{-4}$)		16QAM (BER $< 10^{-3}$)	
		NLMS	IPNLMS	NLMS	IPNLMS	NLMS	IPNLMS
200 m	0	0	0	0	0	0	0
(45 packets	1	14	26	7	8	3	12
in total)	2	34	40	16	24	8	25
	3	42	43	20	26	14	32
	4	42	43	24	31	19	35
	5	43	44	26	31	20	35
1000 m	0	0	3	0	0	0	0
(19 packets	1	10	16	7	7	4	7
in total)	2	15	16	8	8	8	13
	3	16	16	8	8	10	13
	4	16	17	8	8	11	13
	5	16	17	8	8	11	13

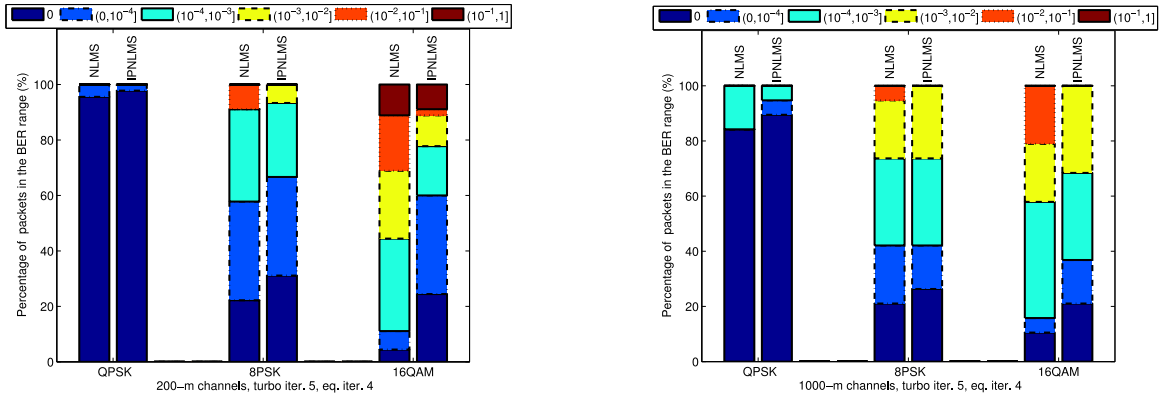

(a) (b)

Fig. 8. Detection results of the two-transducer MIMO transmission after 5 turbo iterations. (a) Results of the 200-m channels. (b) Results of the 1000-m channels.

The step size μ of the adaptive algorithms was set to be exponentially decaying with each data reuse iteration as in [4], [11], and the decaying factor was set as $\beta = 0.9$. The initial step size was chosen as $\mu = 1$ during the training period, and decreased to $\mu = 0.1$ at the DD mode. The choices of $K_1 = 100$, $K_2 = 50$, and $K_3 = K_4 = 50$ are used for the feedforward filter and the SIC filter, respectively, in this particular experiment.

The maximum number of equalizer iteration (or data reuse) was set as 4. Other relevant parameters in the adaptive algorithm were set as $\delta_{\text{NLMS}} = 0.01, \delta_{\text{IPNLMS}} = 5 \times 10^{-5}, \epsilon = 0.01$, and $\alpha = 0$.

B. Experimental Results

The results for the 200-m and 1000-m transmissions are presented. For the 200-m transmission, 30 S3 files and 15 S4 files described in Table I were recorded in two days during the experiment. Each file contains one burst as shown above, and all 45 files were processed. For the 1000-m transmission, 34 data files were recorded during the trial but only 19 of them are valid. The 19 valid files including eight S5 files and eleven S6 files, were all processed.

1) Results on the Two-Transducer MIMO Transmission: In this section, the processing of the two-transducer MIMO data is discussed. Table III provides a summary of the results, and the figure of merit is the number of packets achieving a specific bit error rate (BER) level. From the table, the following observations are made: First, the effectiveness of the turbo equalization is clearly shown, as the detection performance increases with the number of turbo iterations; second, the proposed SD-ATEQ with either NLMS or IPNLMS manifests fast convergence, since most packets achieve the specified BER performance within $3 \sim 4$ turbo iterations; third, the IPNLMS-based SD-ATEQ exhibits better performance than the NLMS-based SD-ATEQ, and the performance gain tends to increase with the modulation level. With QPSK or 8PSK modulations, the NLMS achieves comparable performance to the IPNLMS while at lower complexity, thus is a desired choice for practical use. However with 16QAM modulation, the IPNLMS achieves considerable performance gain over the NLMS so is more preferred.

Fig. 8 provides a graphical presentation of the final detection results (after five turbo iterations) in Table III, where different color bars correspond to the different BER ranges. It is easy to see that for the QPSK modulation, the NLMS and the IPNLMS achieve similar performance for both the 200-m and the 1000-m transmissions. For the 8PSK modulation, the IPNLMS is slightly better than the NLMS. However with the 16QAM modulation, the performance gap between the NLMS and IPNLMS is substantial. For example, the 200-m result shows the percentage of the packets with BER $< 10^{-4}$ increases from 11.1% for the NLMS to 60% for the IPNLMS after five turbo iterations.

Finally, performance analysis is provided for the proposed adaptive equalization via the mean square error (MSE) curve. For a given turbo iteration, the MSE of the nth transmit stream at the $(t+1)$th equalization iteration is estimated via a leaky integrator as [12], [13]

$$\text{MSE}_{n,k+1}^{t+1} = \lambda \text{MSE}_{n,k}^{t+1} + (1-\lambda)|e_{n,k}^{t+1}|^2 \tag{26}$$

where $k = 1, \ldots, K_b$, $e_{n,k}^{t+1} = \breve{x}_{n,k}^{t} - \hat{x}_{n,k}^{t+1}$ and λ is set as 0.99. It is noted that $\text{MSE}_{n,1}^{t+1} = \text{MSE}_{n,K_b+1}^{t}$, $e_{n,k}^{0} = Q(\hat{x}_{n,k}^{0}) - \hat{x}_{n,k}^{0}$ when $N_{\text{iter}} = 0$, and $e_{n,k}^{0} = \bar{x}_{n,k} - \hat{x}_{n,k}^{0}$ when $N_{\text{iter}} > 0$. In Fig. 9, the MSE curves obtained in the detection of 200-m 2×6 MIMO packet with 8PSK and 16QAM modulations are presented, for the first and the third turbo iteration. Obviously, the MSE gaps between the NLMS and the IPNLMS tend to decrease with the number of equalization iterations. Even though, for the 16QAM modulation, there is still nonnegligible 2-dB difference between the IPNLMS and the NLMS, after multiple equalizer iterations. This observation matches the BER results in Table III.

2) Results on the MIMO Transmission with More Than Two Transducers: This section presents the processing results for 3×12 and 4×12 MIMO transmission. Compared with the two-transducer transmission, the detection gets more difficult with more concurrent transmission streams, due to the increased cochannel interference. In Fig. 10, the 3×12 results of the 1000-m transmission are presented. With a 22.73% training overhead, both the NLMS and the IPNLMS-based SD-ATEQs detected successfully most QPSK packets with BER $< 10^{-4}$. Specifically, with the IPNLMS algorithm, 84.2% of the packets achieve BER $< 10^{-4}$ and the remaining packets have the BER $< 10^{-3}$. As to the 8PSK packets, 89.5% of them achieve satisfactory performance with BER $< 10^{-2}$ with the IPNLMS

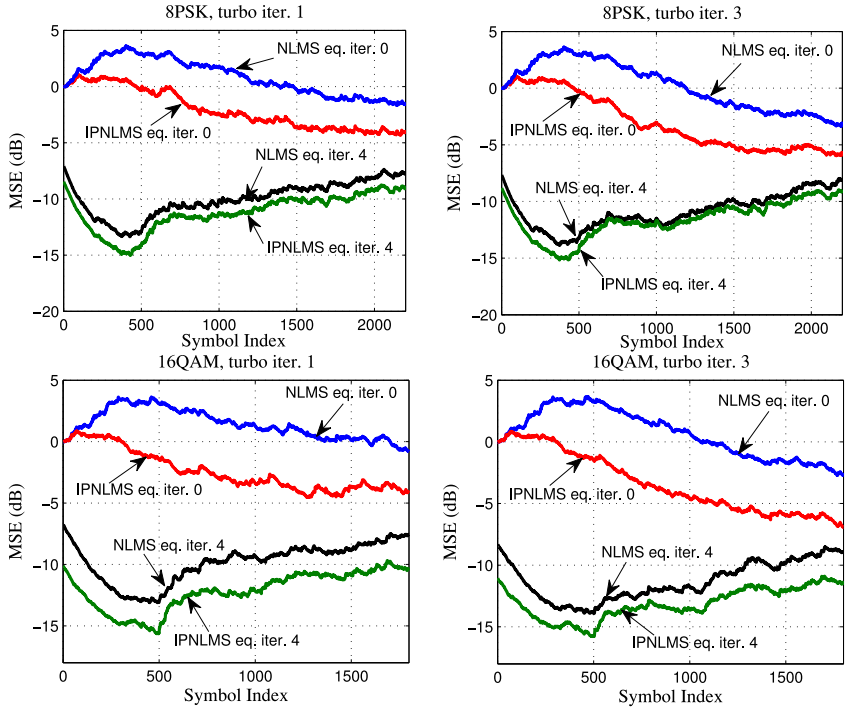

Fig. 9. MSE curves of the 2×6 MIMO detection with 8PSK and 16QAM modulations (200-m channel).

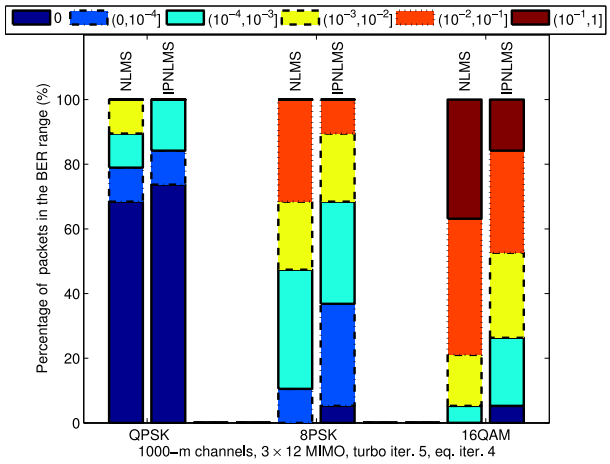

Fig. 10. Detection results of the 3×12 MIMO transmission after five turbo iterations (1000-m channel).

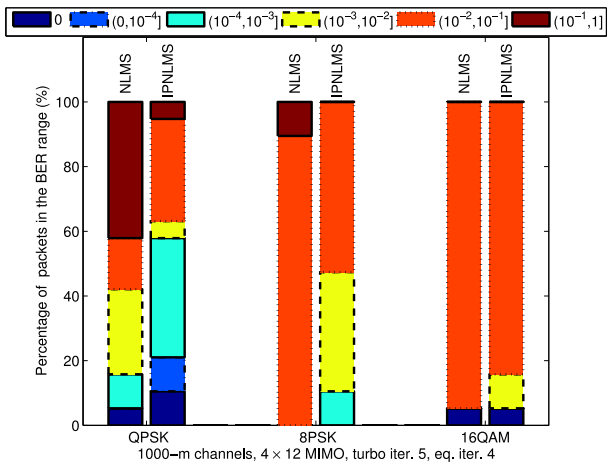

Fig. 11. Detection results of the 4×12 MIMO transmission after five turbo iterations (1000-m channel).

algorithm, at a 27.78% training overhead. The training overhead for the 16QAM modulation was increased to 33.3%. With the IPNLMS-based SD-ATEQ, 52.6% 16QAM packets achieve the BER $< 10^{-2}$, and 31.6% packets reach the BER level of 10^{-2}.

The results of the 4×12 MIMO transmission are next presented in Fig. 11, where the training overheads have been increased to 27.78%, 41.76%, and 47.6% for QPSK, 8PSK, and 16QAM, respectively. For QPSK modulation, the IPNLMS algorithm still works decently. Specifically, 57.9% QPSK packets achieve satisfactory performance with BER $< 10^{-3}$, and only one packet fails with BER $> 10^{-1}$. The detection results for 8PSK and 16QAM modulations are not as satisfactory as those for the QPSK modulation, even when a higher training overhead was used. A closer look at the detection results reveals the performance bottleneck lies in the third transmit stream, whose signal strength is pretty weak on the receive side.

3) Comparison Between the Proposed SD-ATEQ and the HD-ATEQ: It is found that the HD-ATEQ experienced convergence issues in the processing of 8PSK and 16QAM packets, due to the catastrophic effect of the EP. Even with QPSK modulation, the NLMS-based HD-ATEQ did not converge as also observed in [4]. Therefore, the comparison between the proposed SD-ATEQ and the HD-ATEQ is limited to the two-transducer MIMO transmission with QPSK modulation and the IPNLMS algorithm. The comparison is shown in Fig. 12 for the 200-m transmission. Note that we plotted the packets without error on the line of BER $= 10^{-5}$ in Fig. 12(b) for better observation. Obviously, the SD-ATEQ outperforms the HD-ATEQ.

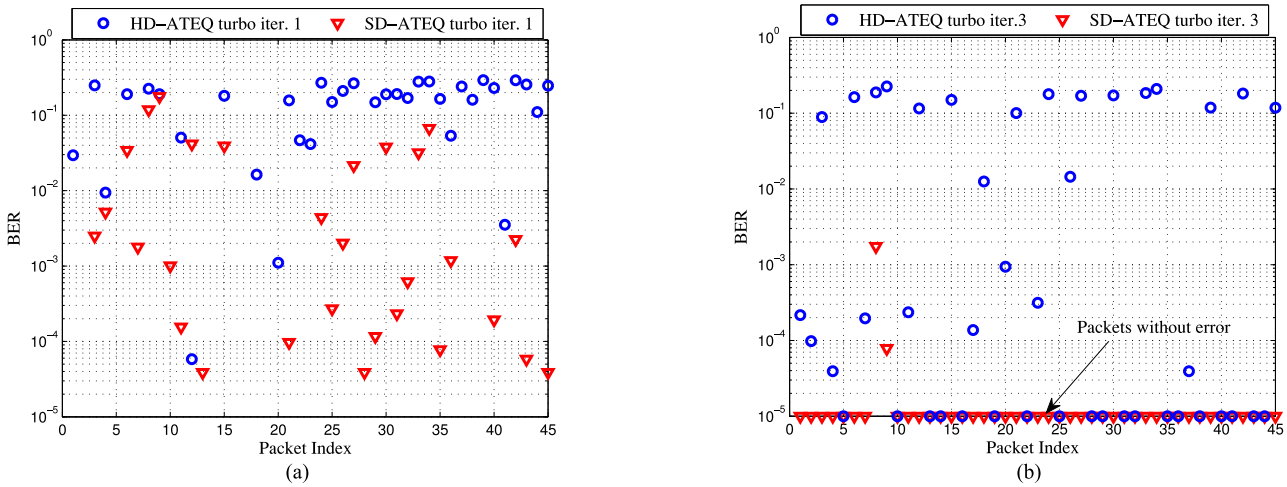

Fig. 12. BER comparison between the SD-ATEQ and the HD-ATEQ for 2×6 MIMO transmission (200-m channels). (a) Comparison after one turbo iteration. (b) Comparison after three turbo iterations.

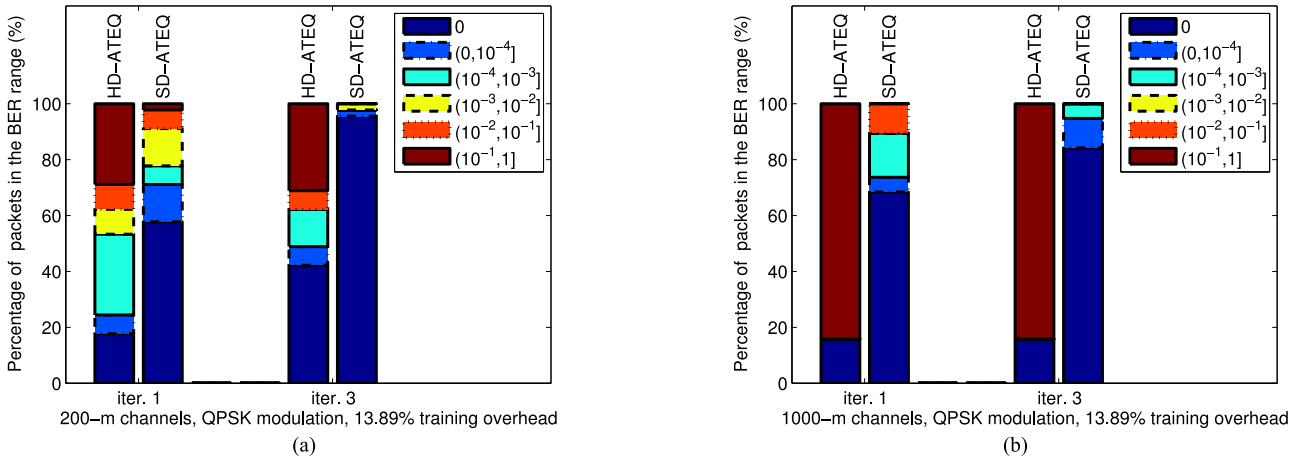

Fig. 13. BER range comparison between the SD-ATEQ and the HD-ATEQ after one and three turbo iterations for 2×6 MIMO transmission. (a) Comparison in the 200-m channels. (b) Comparison in the 1000-m channels.

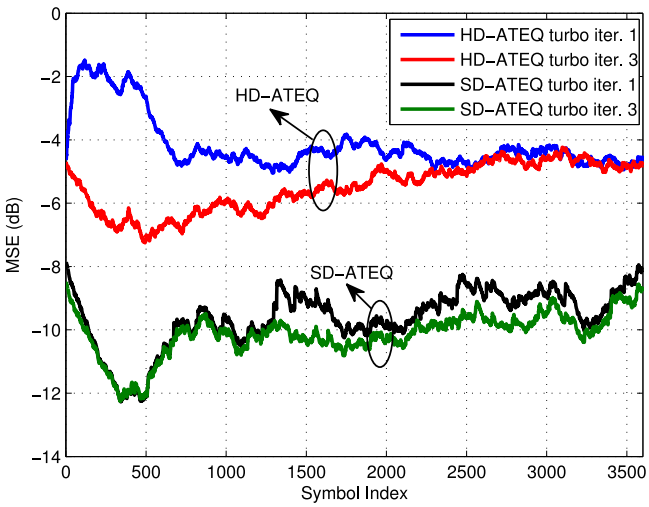

Fig. 14. MSE comparison between the SD-ATEQ and the HD-ATEQ for 2×6 MIMO transmission (200-m channels).

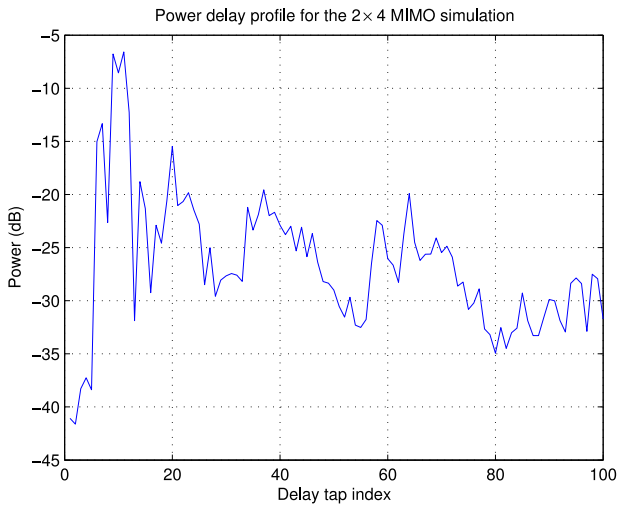

Fig. 15. Estimated power delay profile from experimental channels used for simulations.

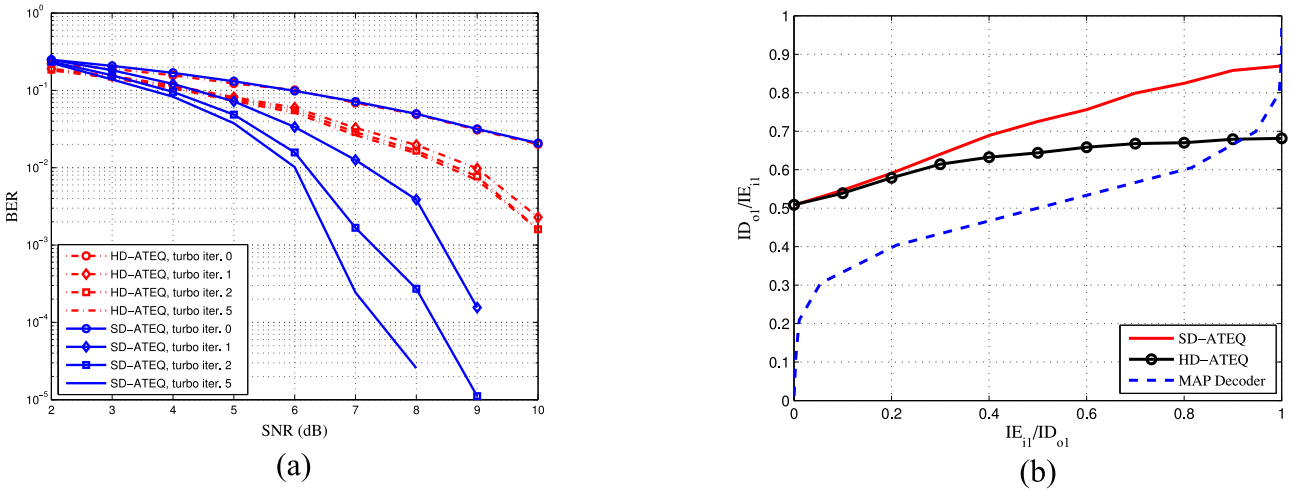

Fig. 16. Simulation results of the proposed SD-ATEQ and the HD-ATEQ in 2×4 MIMO channels with QPKS modulation. (a) BER curves (b) EXIT chart (SNR $=$ 8 dB).

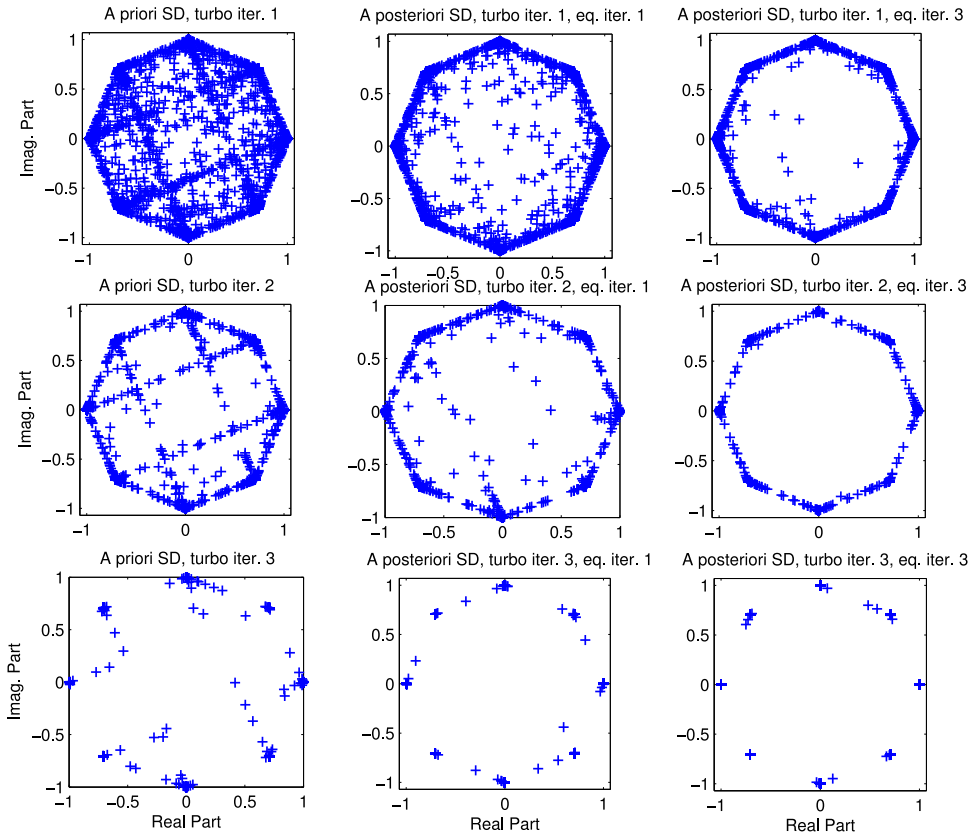

Fig. 17. Evolution of SDs.

dramatically. After three turbo iterations, 43 packets achieve zero BER by using the SD-ATEQ. On the contrary, the detection still fails for 15 packets with BER larger than 10^{-1} when the HD-ATEQ is adopted.

In Fig. 13, the detection results of the 200 and 1000-m transmissions are compared in terms of the percentages of different BER ranges. After one turbo iteration, 71.1% and 73.3% of packets achieve BER $< 10^{-4}$ for the 200-m channel and the 1000-m channel, respectively, with the proposed SD-ATEQ. With three turbo iterations, the SD-ATEQ successfully detected 97.8% 200-m packets and 94.8% 1000-m packets with BER $< 10^{-4}$ (most of these packets achieved zero BER). However with the HD-ATEQ, there are still 31.1% 200-m packets and 84.2% 1000-m packets failed with BER $> 10^{-1}$. This comparison again demonstrates the superiority of the proposed SD-ATEQ over the HD-ATEQ.

Finally, the comparison in terms of MSE is presented in Fig. 14.

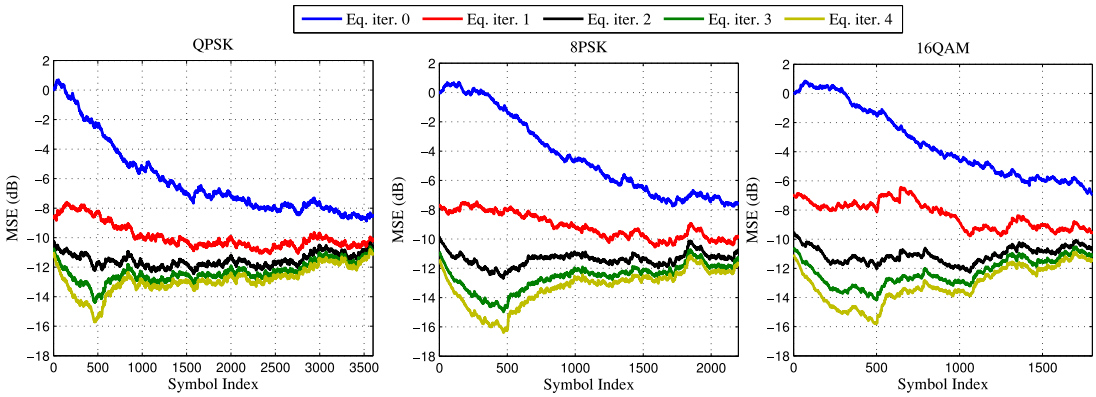

Fig. 18. MSE evolution of the IPNLMS-based SD-ATEQ.

From the figure, the difference in MSE between the proposed SD-ATEQ and the HD-ATEQ can be more than 5 dB. Further, the SD-ATEQ converges faster than the HD-ATEQ, as shown by the gap between the first and the third turbo iteration.

We also compare the performance of the proposed SD-ATEQ with the existing HD-ATEQ based on simulations. In the simulation, we consider a 2×4 MIMO systems with QPSK modulation, where each subchannel is a frequency selective Raleigh fading channel. The fading channels are generated with the power delay profile described in Fig. 15, which is estimated from the experimental channels. The rate $1/2$ convolutional code with generator polynomial [17, 13] in octal notation is used in the simulation. The data payload partition scheme is the same as one in the experiment and the training overhead is set as 20%. The normalized Doppler frequency is chosen as 1.28×10^{-4}, which corresponds to the maximum doppler shift (5 Hz) estimated from the experimental data.

The BER and extrinsic information transfer chart (EXIT) [24] simulation results are demonstrated in Fig. 16(a) and (b). Obviously, the SD-ATEQ outperforms the HD-ATEQ, which is consistent with the results in the experiment. From both the BER and EXIT curves, we can also find the early convergence of the HD-ATEQ in the tough time varying MIMO channels, which is also observed in the experimental data processing.

4) Evolutional Behavior of the Proposed SD-ATEQ: The performance gain brought by the turbo iteration of the SD-ATEQ, has been demonstrated in Table III. In this section, the evolutional behavior of the SD-ATEQ is elaborated in more details.

In Fig. 17, the quality evolution of the SDs is presented by using 8PSK packet as an example. Each row shows the quality evolution at different equalizer iterations for a given turbo iteration, and each column demonstrates the quality evolution at different turbo iterations for a given equalizer iteration. Obviously, the quality of the SDs increases with the number of equalizer iterations and the number of turbo iterations, as expected. It is also clearly shown that the *a posteriori* SDs provide better fidelity than the *a priori* SDs due to the extra information gleaned over the equalization iterations.

In Fig. 18, the evolutional behavior of the IPNLMS-based SD-ATEQ is demonstrated by using MSE as the figure of merit. For each subfigure, the number of turbo iterations is fixed as 3, and the number of equalization iterations varies from 0 to 4.

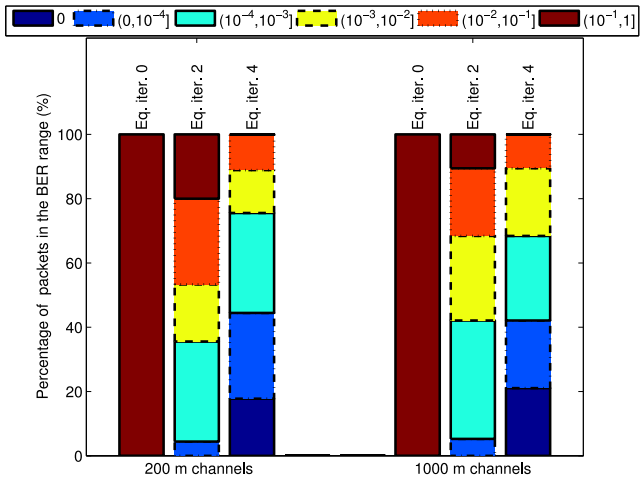

Fig. 19. Performance evolution of the NLMS-based SD-ATEQ (2×6 MIMO, 8PSK, 22.73% training overhead).

Obviously, the MSE decreases consistently with the increase in the equalization iterations, regardless of the modulation. With four equalization iterations, the performance gain achieved can be up to 14 and 6 dB during the training phase and the DD phase, respectively. The results with the NLMS-based SD-ATEQ are very similar thus omitted for brevity.

In Fig. 19, the performance evolution of the NLMS-based SD-ATEQ with different numbers of equalization iterations is shown for the 8PSK packets, where the number of turbo iteration has been fixed as three. Obviously, the detection fails (the BERs of all the packets are above 10^{-1}) without using any equalizer iteration. The performance keeps increasing with the increase in the number of equalizer iterations.

V. Conclusion

An SD-ATEQ scheme was proposed for MIMO UWA communications. The data reuse technique was adopted such that the adaptive equalizer itself performs iterative symbol detection, enabling the usage of *a posteriori* SDs for the equalizer adaptation and the SIC. Attributed to the better fidelity of the *a posteriori* SDs as compared with the *a priori* SDs employed in the existing ATEQ, the proposed scheme not only provided robust detection performance but was very efficient in terms of spectral utilization and processing delay. Therefore, it is a good

candidate for practical use. The proposed scheme was tested by the experimental data collected in the SPACE08 undersea experiment and showed powerful detection capability. It worked successfully in MIMO transmission with multilevel modulations and more than two concurrent transmit streams, which is not found in the existing literature.

REFERENCES

[1] M. Stojanovic and J. Preisig, "Underwater acoustic communication channels: Propagation models and statistical characterization," *IEEE Commun. Mag.*, vol. 47, no. 1, pp. 84–89, Jan. 2009.

[2] T. C. Yang, "A study of spatial processing gain in underwater acoustic communications," *IEEE J. Ocean. Eng.*, vol. 32, no. 3, pp. 689–709, Jul. 2007.

[3] R. Otnes and M. Tuchler, "Iterative channel estimation for turbo equalization of time-varying frequency-selective channels," *IEEE Trans. Wireless Commun.*, vol. 3, no. 6, pp. 1918–1923, Nov. 2004.

[4] Z. Yang and Y. R. Zheng, "Iterative channel estimation and turbo equalization for multiple-input–multiple-output underwater acoustic communications," *IEEE J. Ocean. Eng.*, vol. 41, no. 41, pp. 232–242, Jan. 2016.

[5] J. Tao, Y. R. Zheng, C. Xiao, and T. Yang, "Robust MIMO underwater acoustic communications using turbo block decision-feedback equalization," *IEEE J. Ocean. Eng.*, vol. 35, no. 4, pp. 948–960, Oct. 2010.

[6] A. Rafati, H. Lou, and C. Xiao, "Soft-decision feedback turbo equalization for LDPC-coded MIMO underwater acoustic communications," *IEEE J. Ocean. Eng.*, vol. 39, no. 1, pp. 90–99, Mar. 2014.

[7] W. Duan and Y. R. Zheng, "Bidirectional soft-decision feedback turbo equalization for MIMO systems," *IEEE Trans. Veh. Technol.*, vol. 65, no. 7, pp. 4925–4936, Jul. 2016.

[8] B. Peng and H. Dong, "Application of turbo equalization in ppc underwater acoustic communication," in *Proc. MTS/IEEE OCEANS Conf.*, San Diego, CA, USA, Sep. 2013, pp. 1–4.

[9] P. A. Van Walree and G. Leus, "Robust underwater telemetry with adaptive turbo multiband equalization," *IEEE J. Ocean. Eng.*, vol. 34, no. 4, pp. 645–655, Oct. 2009.

[10] L. Cannelli, G. Leus, H. Dol, and P. van Walree, "Adaptive turbo equalization for underwater acoustic communication," in *Proc. MTS/IEEE OCEANS Conf.*, Bergen, Norway, 2013, pp. 1–9.

[11] J. W. Choi, T. J. Riedl, K. Kim, A. C. Singer, and J. C. Preisig, "Adaptive linear turbo equalization over doubly selective channels," *IEEE J. Ocean. Eng.*, vol. 36, no. 4, pp. 473–489, Oct. 2011.

[12] C. Laot, N. Beuzeulin, and A. Bourre, "Experimental results on MMSE turbo equalization in underwater acoustic communication using high order modulation," in *Proc. MTS/IEEE OCEANS Conf.*, Seattle, WA, USA, Sep. 2010, pp. 1–6.

[13] C. Laot and R. L. Bidan, "Adaptive MMSE turbo equalization with high-order modulations and spatial diversity applied to underwater acoustic communications," in *Proc. 11th Eur. Wireless Conf. Sustain. Wireless Technol.*, Apr. 2011, pp. 1–6.

[14] M. Qingwei, H. Jianguo, H. Jing, H. Chengbing, and M. Chuang, "An improved direct adaptive multichannel turbo equalization scheme for underwater communications," in *Proc. MTS/IEEE OCEANS Conf.*, Yeosu, South Korea, May 2012, pp. 1–5.

[15] A. Yellepeddi and J. C. Preisig, "Adaptive equalization in a turbo loop," *IEEE Trans. Wireless Commun.*, vol. 14, no. 9, pp. 5111–5122, Sep. 2015.

[16] S. Roy and J. J. Shynk, "Analysis of the data-reusing LMS algorithm," in *Proc. 32nd Midwest Symp. Circuits Sys.*, vol. 2, Aug. 1989, pp. 1127–1130.

[17] J. Tao, "Single-carrier frequency-domain turbo equalization with various soft interference cancellation schemes for MIMO systems," *IEEE Trans. Commun.*, vol. 63, no. 9, pp. 3206–3217, Sep. 2015.

[18] M. Tuchler, R. Koetter, and A. C. Singer, "Turbo equalization: Principles and new results," *IEEE Trans. Commun.*, vol. 50, no. 5, pp. 754–767, May 2002.

[19] M. Tuchler, A. C. Singer, and R. Koetter, "Minimum mean squared error equalization using *a priori* information," *IEEE Trans. Signal Process.*, vol. 50, no. 3, pp. 673–683, Mar. 2002.

[20] H. Lou and C. Xiao, "Soft-decision feedback turbo equalization for multilevel modulations," *IEEE Trans. Signal Process.*, vol. 59, no. 1, pp. 186–195, Jan. 2011.

[21] S. Haykin, *Adaptive Filter Theory*, 4th ed. Upper Saddle River, NJ, USA: Prentice-Hall, 2002.

[22] D. L. Duttweiler, "Proportionate normalized least-mean-squares adaptation in echo cancelers," *IEEE Trans. Speech, Audio Process.*, vol. 8, no. 5, pp. 508–518, Sep. 2000.

[23] A. J. Paulraj, D. A. Gore, R. U. Nabar, and H. Bölcskei, "An overview of MIMO communications-a key to gigabit wireless," in *Proc. IEEE*, vol. 92, no. 2, pp. 198–218, Feb. 2004.

[24] S. Ten Brink, "Convergence behavior of iteratively decoded parallel concatenated codes," *IEEE Trans. Commun.*, vol. 49, no. 10, pp. 1727–1737, Oct. 2001.

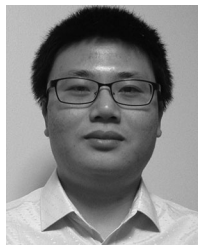

Weimin Duan was born in China in 1987. He received the B.S. degree in electrical engineering and M.S. degree in underwater acoustic engineering from Harbin Engineering University, Harbin, China, in 2010 and 2013, respectively and the Ph.D. degree in electrical engineering from Missouri University of Science and Technology, Rolla, MO, USA, in 2016.

He is currently with Qualcomm Research, San Diego, CA, USA. His research interests include MIMO signal processing, iterative detection, and wireless and underwater acoustic communications.

Jun Tao (S'10–M'10) received the B.S. and M.S. degrees in electrical engineering from the Department of Radio Engineering, Southeast University, Nanjing, China, in 2001 and 2004, respectively, and the Ph.D. degree in electrical engineering from the Department of Electrical and Computer Engineering, University of Missouri, Columbia, MO, USA, in 2010.

From 2004 to 2006, he was a System Design Engineer in Realsil Microelectronics, Inc., (a subsidiary of Realtek), Suzhou, China. From 2011 to 2015, he was a Senior System Engineer with Qualcomm, Inc., Boulder, CO, USA, working on the baseband algorithm and architecture design for the UMTS/LTE modem. Since April 2016, he has been a Full Professor in the School of Information Science and Engineering, Southeast University, Nanjing, China. His research interests lie in the general areas of wireless cellular communications and underwater acoustic communications, including channel modeling and estimation, turbo equalization, adaptive filtering, and baseband algorithm design for practical systems conforming to the UMTS and LTE standards.

Y. Rosa Zheng (M'03–SM'07–F'15) received the B.S. degree in electrical engineering from the University of Electronic Science and Technology of China, Chengdu, China, in 1987, the M.S. degree in electrical engineering from Tsinghua University, Beijing, China, in 1989, and the Ph.D. degree from Carleton University, Ottawa, ON, Canada, in 2002.

From January 2003 to April 2005, she was a Natural Sciences and Engineering Research Council Postdoctoral Fellow with the University of Missouri, Columbia, MO, USA. Since Fall 2005, she has been with the Department of Electrical and Computer Engineering, Missouri University of Science and Technology, Rolla, MO, USA, where she is currently a Professor. Her research interests include array signal processing, wireless communications, and wireless sensor networks. Dr. Zheng was a Technical Program Committee Member for many IEEE international conferences, including the IEEE Vehicular Technology Conference, the IEEE Global Communications Conference (IEEE GLOBECOM), the IEEE International Conference on Communications (IEEE ICC), and the IEEE Wireless Communications and Networking Conference. She was a Wireless Communications Symposium Cochair of the IEEE GLOBECOM in 2012 and the IEEE ICC in 2014. She was also an Associate Editor of the IEEE TRANSACTIONS ON WIRELESS COMMUNICATIONS during 2006–2008. She is currently as an Associate Editor of the IEEE TRANSACTIONS ON VEHICULAR TECHNOLOGY. She received the U.S. National Science Foundation CAREER Award in 2009.